A tractable molecular theory of flow in strongly inhomogeneous fluids

I. Bitsanis, T. K. Vanderlick, M. Tirrell, and H. T. Davis
Department of Chemical Engineering and Materials Science, University of Minnesota, Minneapolis, Minnesota 55455

(Received 14 March 1988; accepted 16 May 1988)

A recently introduced model is used to study several flows in fluids with large density variations over distances comparable to their molecular dimensions (strongly inhomogeneous fluids). According to our model, the local average density model (LADM), local viscosity coefficients can be assigned at each point in a strongly inhomogeneous fluid and the stress tensor retains its Newtonian form provided that the properly defined local viscosities are used. The model has been previously shown to agree with the results of molecular dynamics simulations on diffusion and flow properties in plane Couette flow. Application of this model requires determination of the molecular density profiles in the flow region. Using a successful closure for the pair distribution function, we solve the Yvon–Born–Green (YBG) equation of fluid structure in order to determine the density profiles of a fluid confined between planar micropore walls only a few molecular diameters apart. The fluid confinement produces a strongly inhomogeneous structure. Subsequently we apply LADM to set up the fluid mechanical equations for Couette flow, Poiseuille flow, and squeezing flow between parallel plates. With the use of the YBG theoretical density profiles we solve the flow equations and predict velocity profiles, stress distributions, and effective viscosities. The dependence of these quantities on the fluid inhomogeneity is described. The effective viscosity of strongly inhomogeneous fluids is found to be quite sensitive to the nature of the flow. Our squeezing flow analysis provides a first explanation of recent experimental findings on the effective viscosity of simple fluids confined in very narrow spaces.

I. INTRODUCTION

In the interfacial zone between coexisting bulk fluid phases, in fluid near a solid wall or in fluid within microscopic pores, the fluid density is strongly inhomogeneous. The strong density variation has been predicted from microscopic models of fluid structure,[1] has been observed in many molecular simulations,[2,3] and has been deduced experimentally.[4]

There has been considerable progress in our understanding of the equilibrium properties of interfacial fluids during the last decade.[5–8] Little has been done, however, towards understanding the transport and flow behavior of these systems. Contrary to bulk fluids, interfacial fluids exhibit strong density variations on a microscopic, molecular scale. This fact introduces serious conceptual and operational difficulties in the description of their transport behavior. In particular, the lack of uniformity on a molecular scale makes the traditional microscopic identification of the mass flux, stress tensor, and energy flux inappropriate[9] causing in this way the failure of the usual microscopic definition of local transport coefficients.

An alternative starting point is the generalization of Enskog's kinetic theory to fluids with strong density inhomogeneities over molecular distances. This approach has been pursued recently by Davis and co-workers.[10–13] The constitutive equations resulting from such an approach are different and more complicated than those of bulk fluids due to the inherent anisotropy of the strongly inhomogeneous medium. The corresponding hydrodynamic equations, therefore, are much more complex than the usual Navier–Stokes equations, which makes their application tedious to all but the simplest flows.

Recently, we completed a series of molecular dynamics simulations that investigated the effect of strong density variations over molecular distances on the flow behavior of simple fluids.[14] We simulated a fluid consisting of molecules that interact via pairwise additive, spherically symmetric forces of the Lennard-Jones type. The fluid molecules were confined between planar micropore walls that exerted forces on them. The pore width was 5.4 molecular diameters. By employing a nonequilibrium molecular dynamics technique[15] a constant shear rate was imposed upon the fluid slab, thereby simulating plane Couette flow.

The effect of the density inhomogeneity on the flow behavior is demonstrated in Fig. 1 taken from Ref. 14. Instead of the linear velocity profile that would be developed in a homogeneous fluid, a clearly nonlinear velocity profile is observed. Superimposed on the velocity profile is the density profile. We see that the density profile is indeed strongly inhomogeneous and exhibits substantial fluid layering. Some kind of correlation between density and velocity is already apparent from Fig. 1. The regions of low slope of the velocity profile next to the walls correspond to the two high density regions, while the high slope in the center of the pore corresponds to the much lower densities of this region. Furthermore, these results show that the effective shear viscosity and the pore average shear stress of the micropore fluid are much lower than the corresponding homogeneous fluid values (see Table I for the units of the various quantities and Table II). These simulation results can be regarded as "experimental findings." Our model fluid as shown by Bitsanis

 0021-9606/88/173152-11$02.10

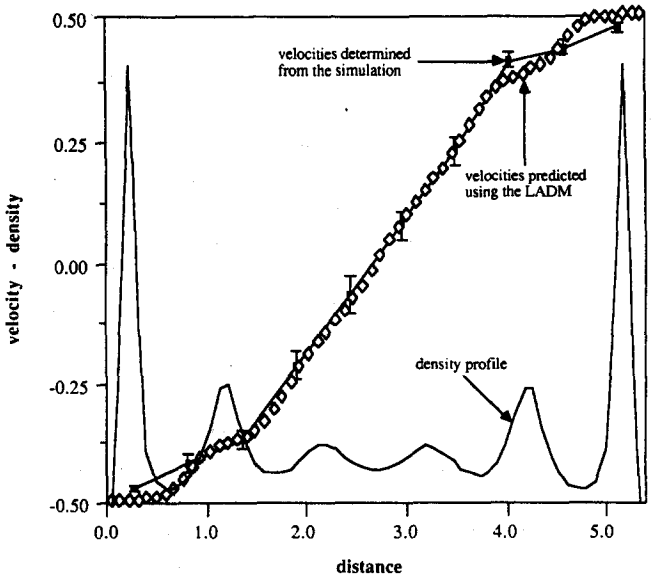

FIG. 1. Density and velocity profiles for the micropore fluid simulated by Bitsanis *et al.* (Ref. 16). The open squares are the theoretical velocities, predicted by LADM.

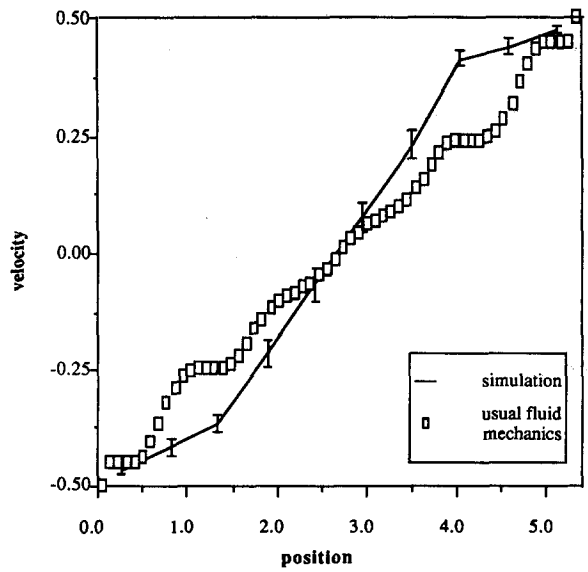

FIG. 2. Comparison of the velocity profile predicted by usual hydrodynamics (point function dependence of the local transport coefficients on the density) with the simulation results (Ref. 14).

et al.[14] accurately reproduces the flow behavior of a real homogeneous fluid in the sense that if the pore walls (and hence the density inhomogeneity) are removed and a constant shear rate is imposed upon the homogeneous fluid a perfectly linear velocity profile is developed and the simulation values for the effective shear viscosity and the diffusivity are identical with the experimental values for liquid argon within the statistical uncertainty of the simulation results (less than 4%).

The correlation between the density and the velocity profiles in Fig. 1 suggests that the introduction of local viscosities might be useful for the description of flow in strongly inhomogeneous fluids, despite the conceptual difficulties associated with their definition. According to usual hydrodynamics local transport coefficients can be assigned at each point inside an inhomogeneous fluid. These are the same as the transport coefficients of a homogeneous fluid at the local density, i.e., they are point functions of the density. Usual hydrodynamics are of course applicable only if the fluid density, despite its macroscopic variation, hardly changes over molecular distances. Let us ignore these limitations, however, and for the sake of argument take the point function definition of the local transport coefficients literally and apply it in order to predict the velocity profile and the effective viscosity of the strongly inhomogeneous fluid with the density profile shown in Fig. 1. The results of such a calculation are shown in Fig. 2 and Table II. The comparison between these predictions and the simulation results is rather disappointing. It appears that the effects of strong density inhomogeneities on the flow and transport behavior are much weaker than what they would have been, had the local transport coefficients been literally point functions of the density.

Based on these considerations, Bitsanis *et al.*[14] presented a model, the local average density model (LADM), that leads to tractable equations for the prediction of the flow behavior and the transport coefficients of strongly inhomogeneous fluids. The agreement between the LADM predictions and the simulation results was found to be surprisingly good[13,14] as it can be seen from Fig. 1 and Table II. Furthermore, LADM agreed well with more rigorous but more complex kinetic theoretical results of Davis *et al.*[10–13]

It seems, therefore, that LADM provides an adequate description of transport and flow in strongly inhomogeneous fluids, yet it retains most of the simplicity of usual hydrodynamics. Of course, the application of LADM requires the knowledge of the fluid density profiles. The important developments in the equilibrium theories of strongly inhomogeneous fluids[5–8] allow an almost quantitative prediction of the equilibrium density profiles.

The fluid density profile under flow can in principle be different from the equilibrium one. The simulations of Bitsanis *et al.*,[14] however, demonstrated that flow does not affect sensibly the density profile even for shear rates orders of magnitude higher than those encountered in usual flow situations. This is an important point, since it allows the decoupling of the problems of density profile determination and flow description.

The simulation findings[14] combined with the theoretical advances[5–8] allow for the first time a theoretical prediction of the flow behavior of strongly inhomogeneous fluids. The means of doing fluid mechanics in strongly inhomogeneous fluids are now available and the first objective of this article is to demonstrate their use by actually solving typical flow problems. The flows that will be studied (Couette flow, Poiseuille flow, and squeezing flow between parallel plates) are of considerable importance because they occur in systems of practical interest (pressure driven flow in micropore solids) or they have been used in relevant experiments (squeezing flow between the solid surfaces of the surface forces apparatus[16,17]).

The second objective is to provide information on the

effects of strong density inhomogeneities in different flow situations, to demonstrate that the failure of a continuum description of the flow occurs at different points for different flows, and to show that the effect of fluid structure on important material properties, like the effective viscosity, depends strongly on the type of flow.

Finally, our third objective is to provide a molecular level rationalization of recent puzzling experimental measurements of the effective viscosity of molecularly thin liquid films.[16,17] Hopefully, this rationalization will allow the design of more revealing experiments on the flow and transport behavior of strongly inhomogeneous fluids.

The rest of this paper has been organized as follows: In Sec. II the LADM for strongly inhomogeneous fluids is presented. This model provides a constitutive equation which along with the knowledge of the density profile, enables us to set up the fluid mechanical equations. In this section we also review the molecular theory that leads to the prediction of the density profiles and which motivated the development of LADM. In Sec. III we set up and solve the fluid mechanical equations for plane Couette flow, Poiseuille flow, and squeezing flow between parallel plates in strongly inhomogeneous fluids confined between planar micropore walls. In Sec. IV the velocity profiles and the effective viscosities for these flows are presented and their dependence on the fluid structure is demonstrated and discussed. In the same section we discuss the relevance of our squeezing flow calculations with the experimental results of Chan and Horn[16] providing in this way a first molecular level rationalization of these results and an explanation for their apparent discrepancy with the results of Israelachvili.[17]

II. THEORY

According to the LADM[14] the local value of the transport coefficient at the position $\mathbf{r}$ inside a strongly inhomogeneous fluid is approximated by

$$\lambda(\mathbf{r}) = \lambda^0[\bar{n}(\mathbf{r})] . \tag{2.1}$$

$\lambda^0[\bar{n}(\mathbf{r})]$ is the transport coefficient of a homogeneous fluid at the local average density at the point $\mathbf{r}$. The local average density at $\mathbf{r}$ is defined as the average density inside a sphere with its center at $\mathbf{r}$ and with diameter equal to the diameter of the fluid molecules σ.

$$\bar{n}(\mathbf{r}) = \frac{1}{\pi\sigma^3/6}\int_{R<\sigma/2} n(\mathbf{r}+\mathbf{R})d^3R . \tag{2.2}$$

$n(\mathbf{r})$ is the actual fluid density at the position $\mathbf{r}$.

The constitutive relation according to the LADM retains its Newtonian form:

$$\tau(\mathbf{r}) = \tfrac{1}{2}\eta^0[\bar{n}(\mathbf{r})][\nabla\bar{\mathbf{v}} + \nabla\bar{\mathbf{v}}^T] + \left\{\eta_b^0[\bar{n}(\mathbf{r})] - \tfrac{2}{3}\eta^0[\bar{n}(\mathbf{r})]\right\}\nabla\cdot\mathbf{v}\mathbf{I} , \tag{2.3}$$

where $\bar{\mathbf{v}}$ is the flow velocity, $\nabla\bar{\mathbf{v}}^T$ is the transpose of $\nabla\bar{\mathbf{v}}$, $\eta^0(\bar{n})$ and $\eta_b^0(\bar{n})$ are the shear and bulk viscosity coefficients of the homogeneous fluid at the local average density $\bar{n}$, and $\mathbf{I}$ is the unit second rank tensor.

The LADM, therefore, accounts for the strong density inhomogeneities by the use of transport coefficients that correspond to the coarse grained local average density instead of the actual local density. In the limit of a homogeneous (or weakly inhomogeneous) fluid $\bar{n}(\mathbf{r}) = n(\mathbf{r})$ and one recovers the local equilibrium approximation of usual fluid mechanics.

Despite its *ad hoc* introduction, the use of the local average density is intuitively satisfactory. Heuristically one argues that the transport coefficients in dense fluids are primarily determined by potential interactions between a reference molecule at $\mathbf{r}$ and its nearest neighbors. Some type of averaging is inherent in the very concept of the transport coefficient.[9] The volume over which this averaging is to be performed must be a microscopic volume of molecular dimensions but it is otherwise arbitrary. However, there are several arguments in favor of our specific choice (i.e., a sphere of molecular diameter). The same coarse graining has been used with great success for the pair distribution function of inhomogeneous fluids in equilibrium theories of fluid structure.[8] It has also been shown to give the exact pair correlation function for a system of one-dimensional hard rods.[18] Another reasonable choice for the averaging volume is a sphere with *radius* equal to the molecular diameter. As a matter of fact, this was the first choice used in free energy density functional theories of equilibrium fluid structure.[6,19] Although it might be argued that the employment of such an averaging volume would be closer to the spirit of Fischer and Methfessel's approximation,[8] this larger averaging volume furnished poor predictions for the effective viscosity of the micropore fluid (Table II) without improving the predicted velocity profile over that obtained by the use of the original averaging volume (a sphere with *diameter* equal to the molecular diameter). In Ref. 14 another type of strongly inhomogeneous fluid was studied, namely a fluid confined between two purely repulsive planar walls, which lead to the development of the major density peak at the center of the fluid slab.[14] For this system too, LADM reproduced quantitatively the velocity profile, shear stress, effective viscosity, and average diffusivity. The use of the larger averaging volume (a sphere with radius equal to the molecular diameter) overestimated the effective viscosity by more than 50% and failed to reproduce even qualitatively the simulation velocity profiles.

Perhaps the strongest argument in favor of the LADM is its success in application to plane Couette flow. As it can be seen from Fig. 1 the LADM prediction for the velocity profile agrees almost within the limits of statistical uncertainty with the simulation profile. Bitsanis *et al.*[14] showed that LADM reproduces almost quantitatively the simulation results both for the effective shear viscosity and the pore average diffusivity. A more detailed comparison with extensive diffusivity simulations in micropores of various sizes is also quite satisfactory.[3,13]

To complete the picture one needs a model for the viscosity of homogeneous fluids [see Eq. (2.3)]. The simple, yet fairly successful Enskog model for hard sphere fluids will be used.[20] According to the Enskog theory

$$\eta(n) = \eta^0 bn(Y^{-1} + 0.800 + 0.761Y) , \tag{2.4}$$

where

$\eta^0 = (5\pi m k_B T)^{1/2}/16\pi\sigma^2$ is the hard sphere dilute gas viscosity,
n is the fluid density,
k_B is Boltzmann's constant,
m is the mass of the molecule,
T is the temperature,
σ is the molecular diameter,
$b = 2\pi\sigma^3/3$ is the hard sphere second virial coefficient,
$Y = nbg^0(\sigma;n) = p_{HS}/nk_BT - 1$,
$g^0(\sigma;n)$ is the contact value of the pair correlation function of the hard sphere fluid,
p_{HS} is the pressure of the hard sphere fluid.

One needs an equation of state in order to calculate Y. A reasonably accurate choice for hard sphere fluids is the Carnahan–Starling formula[21]

$$\frac{p_{HS}}{nk_BT} = \frac{1+y+y^3}{(1-y)^3}, \tag{2.5}$$

where $y = \pi n\sigma^3/6$.

When the density profiles are available one can set up the fluid mechanical equation of motion. This equation is similar in form to the Navier–Stokes equation except that the viscosities are *functionals*, not point functions, of the density profile. There are several theories of fluid structure that lead to tractable equations for the density profiles *at equilibrium*. The flow can in principle affect the density profile. Currently there is no theory that assesses the importance of this effect. The molecular dynamics simulations of Bitsanis *et al.*,[14] however, *show that the flow has no detectable effect on the density profile at least up to shear rates orders of magnitude larger than the ones encountered in realistic flow situations* (10^{10}–10^{11} s^{-1}). From this it follows that for usual flow situations the density profile is identical with the equilibrium density profile.

The equilibrium density profiles used as inputs to the analysis that follows were obtained from the Yvon–Born–Green (YBG) theory of inhomogeneous fluids[20] with the Fischer–Methfessel approximation for the pair correlation function.[8] We assume that the particles interact with pairwise additive, spherically symmetric forces whose pair potentials can be approximated by

$$u(s) = u_R(s) + u_A(s), \tag{2.6}$$

where the repulsive part of the potential is

$$u_R(s) = \infty, \quad s<\sigma,$$
$$= 0, \quad s>\sigma, \tag{2.7}$$

and $u_A(s)$ is the continuous, attractive part of the pair potential. The pore walls confining the fluid will be represented by the conservative potential $u^e(\mathbf{r})$. At equilibrium, the density $n(\mathbf{r})$ of the fluid obeys the YBG equation, which is a microscopic force balance,

$$k_BT\nabla n + n\nabla u^e - n\int n(\mathbf{r}+\mathbf{s})g(\mathbf{r},\mathbf{r}+\mathbf{s})\frac{\mathbf{s}}{s}u_A'(s)d^3s + nk_BT\int n(\mathbf{r}+\sigma\mathbf{k})g(\mathbf{r},\mathbf{r}+\sigma\mathbf{k})\sigma^2\mathbf{k}\,d^2k = 0, \tag{2.8}$$

where $g(\mathbf{r},\mathbf{r}')$ is the inhomogeneous fluid pair correlation function, $\mathbf{k}$ is a unit vector lying along the line of centers of a pair of molecules in contact, d^2k denotes an element of solid angle associated with $\mathbf{k}$. The physical meaning of the various terms in the YBG equation is the following: The first term is an entropic force which arises from the density gradients, the second term is an external force (which in our case arises from the wall potential), and the third and the fourth terms are the attractive and repulsive forces, respectively, exerted on molecules at $\mathbf{r}$ from all the other molecules.

Equation (2.8) is exact for fluids whose intermolecular potential is described by Eqs. (2.6) and (2.7). However, in order to compute the density $n(\mathbf{r})$ one must know the relationship between the density distribution and the pair correlation function of inhomogeneous fluids. Such a relationship is not available in general. However, the approximation introduced by Fischer and Methfessel,[8] which in fact inspired our introduction of LADM for describing flow and diffusion, has been shown to give fairly accurate predictions of the density profiles in liquid–vapor and liquid–solid interfaces. It has also been shown that their approximation gives the exact density distribution for one-dimensional hard rods in an external field.[18]

The main assumption of Fischer and Methfessel is that the pair correlation function can be approximated as

$$g(\mathbf{r},\mathbf{r}+\mathbf{s}) = g^0[s;\bar{n}(\mathbf{r}+\tfrac{1}{2}\mathbf{s})], \tag{2.9}$$

where g^0 is the correlation function of homogeneous fluid and $\bar{n}$ is the local average density defined by Eq. (2.2).

This approximation for the pair correlation function renders the YBG equation solvable. However, we shall further simplify the theory by making the van der Waals' structureless fluid approximation ($g = 0, s<\sigma; g = 1, s>\sigma$) in the integral involving the long-ranged force u_A'.[8] The YBG equation thus becomes

$$\nabla\left[k_BT\ln n + u^e + \int n(\mathbf{r}+\mathbf{s})u_A(s)d^3s\right] + k_BT \times \int n(\mathbf{r}+\sigma\mathbf{k})g^0\{\sigma;\bar{n}[\mathbf{r}+(\sigma/2)\mathbf{k}]\}\sigma^2\mathbf{k}\,d^2k = 0. \tag{2.10}$$

Finally, to complete the model, a formula for the contact value of the homogeneous fluid pair correlation function g^0 must be given. We choose the Carnahan–Starling formula

$$g^0(\sigma;\bar{n}) = \frac{1-(\pi/12)\sigma^3\bar{n}}{[1-(\pi/6)\sigma^3\bar{n}]^3} \tag{2.11}$$

known to be quite accurate in hard sphere fluids.[21]

In the calculations to be reported in what follows we shall consider planar systems, i.e., flat pore walls so that $u^e = u^e(z)$ and $n = n(z)$, where z is the distance from a pore wall. In this case Eq. (2.10) can be integrated to give

$$\mu^* = u^e(z) + k_BT\ln n(z) + \int_{-\infty}^{\infty} n(z')\bar{u}_A(z-z')dz' + 2\pi\sigma^2k_BT\int_0^z dz'\int_{-1}^{+1} d\xi\,\xi n(z'+\sigma\xi)g \times[\bar{n}(z'+\tfrac{1}{2}\sigma\xi)], \tag{2.12}$$

where

$$\bar{n}(z) = \frac{6}{\sigma^3} \int_{-\sigma/2}^{\sigma/2} [0.25\sigma^2 - (z - z')^2] n(z') dz' . \tag{2.13}$$

The parameter μ^* is the constant of integration. It plays a role similar to the chemical potential.

The external potential $u^e(z)$ arises from the solid walls at $z = 0$ and $z = D$.

$$u^e(z) = \phi_w(z) + \phi_w(D - z) ,$$

where each wall exerts a 10-4-3 Lennard-Jones potential[21]:

$$\phi_w = \epsilon_w \left[\left(\frac{2}{5}\right)\left(\frac{\sigma_w}{z}\right)^{10} - \left(\frac{\sigma_w}{z}\right)^4 - \frac{\sqrt{2}\sigma_w^3}{3[z + (0.61\sigma_w/\sqrt{2})]^3} \right], \quad z > 0 . \tag{2.14}$$

The fluid–fluid intermolecular potential

$$\bar{u}_A(z) = \int_{-\infty}^{+\infty}\int u^A(s) dy\, dx \tag{2.15}$$

is taken to be

$$\bar{u}_A(z) = -2\pi\epsilon\sigma^2, \quad |z| < \sigma ,$$
$$= -\frac{2\pi\epsilon\sigma^6}{z^4}, \quad |z| > \sigma . \tag{2.16}$$

This corresponds to the attractive part of a "6-∞" Lennard-Jones potential, namely,

$$u^A(s) = -4\epsilon\left(\frac{\sigma}{s}\right)^6, \quad s > \sigma ,$$
$$= 0, \quad s < \sigma .$$

We have chosen the following parameters for our system: $\sigma_w = \sigma$, $\epsilon_w = \epsilon = 0.826\,45\, k_B T$.

The equilibrium density profiles were obtained by solving Eq. (2.12), using Eqs. (2.11) and (2.13) for the pair correlation function. The domain of interest, $0 < z < D$, was discretized uniformly and trapezoidal rule was used to evaluate the integrals. The result is a system of nonlinear, coupled, algebraic equations. Newton's method was used to solve for the nodal values of the density. The domain was discretized finely enough so that the solution changed negligibly with further refinement. A mesh size of 0.05σ was adopted in our calculations.

III. THE FLUID MECHANICAL ANALYSIS

Before setting up and solving the fluid mechanical equations for the three model flows, plane Couette flow, Poiseuille flow, and squeezing flow between parallel circular plates we want to make some comments about the physical realism of the boundary conditions we shall use for the solution of these equations. The planar pore walls we employ are model walls. Apart from the approximate nature of the wall potential, these walls, contrary to most real walls, are perfectly smooth; they lack the roughness of real walls, which in most instances facilitates the sticking of the fluid particles on them and the physical realization of the no-slip boundary condition. The wall potential we employ is the 10-4-3 Lennard-Jones potential [see Eq. (2.14)]. The choice of the proper boundary conditions for flow in strongly inhomogeneous fluids is an important unsolved problem. We do not claim to have solved this problem here. Our choice of boundary conditions (nature of the boundary conditions and position of the no-slip plane) is based on physical intuition and on indirect simulation results which indicate that a no-slip condition is appropriate when a high density layer is located right next to the solid walls.[14] We should note, however, that no hydrodynamic theory is supposed to provide its boundary conditions. In that sense, LADM is equally applicable, no matter what the boundary conditions are, provided that somehow they have been supplied independently.

The density profiles of a Lennard-Jones fluid confined between two 10-4-3 Lennard-Jones pore walls show that up to a distance 0.75–0.8σ the fluid density is practically zero for any wall–wall separation.[3] Furthermore, the simulations of Bitsanis *et al.*[14] indicated that slip is observed next to such walls unless the fluid density is high in the vicinity of the wall. In other words, the answer to the slip–no-slip question for a 10-4-3 Lennard-Jones wall depends on the specific choices of the parameters of the wall potential. Since no fluid exists up to 0.75σ from the wall an analysis of the flow in there is rather meaningless. We decided, therefore, to apply the no-slip boundary conditions at a distance 0.75σ from the walls. One may wish to imagine that in this way we account for slight imperfections of the wall surface that would assure no slip.

For a fluid confined between planar micropore walls, the density varies only in the direction normal to the walls, the z direction. Hence, the local average density and the local viscosity coefficients depend on z only [see Eqs. (2.1) and (2.2)].

A. Plane Couette flow

The flow is in the x direction. Therefore, the macroscopically imposed shear rate $\dot{\gamma}$ is

$$\dot{\gamma} = [v_x(D/2) - v_x(-D/2)]/D . \tag{3.1}$$

The momentum conservation in the z direction simply yields

$$\tau_{zx}(z) = \text{const.} = \bar{\tau}_{zx} , \tag{3.2}$$

where $\bar{\tau}_{zx}$ denotes the pore average shear stress. According to the LADM $\tau_{zx} = -\eta(z)(\partial v_x/\partial z)$, where $\eta(z) = \eta^0[\bar{n}(z)]$. Thus the flow velocity is

$$v_x(z) = \dot{\gamma} \frac{\int_0^z [d\xi/\eta(\xi)]}{(1/D)\int_{-D/2}^{D/2} [d\xi/\eta(\xi)]} \tag{3.3}$$

and the shear stress

$$\tau_{zx}(z) = \bar{\tau}_{zx} = \frac{\dot{\gamma}}{(1/D)\int_{-D/2}^{D/2} [d\xi/\eta(\xi)]} . \tag{3.4}$$

One can identify an effective viscosity by rewriting Eq. (3.4) in a form apparently identical with the homogeneous fluid result:

$$\bar{\tau}_{zx} = \eta_{\text{eff}} \dot{\gamma} . \tag{3.5}$$

Therefore,

$$\eta_{\text{eff}}^{-1} = \frac{1}{D}\int_{-D/2}^{D/2} \frac{d\xi}{\eta(\xi)} . \tag{3.6}$$

Obviously η_{eff} is not a fluid property but depends on the flow as well. It might even depend on the macroscopic observable with which we want to establish the macroscopic connection. These points will be clarified further from the analysis of the remaining two flows.

B. Poiseuille flow

The flow is again in the x direction. The macroscopically imposed pressure gradient is denoted by

$$p_x = \frac{dp}{dx}. \tag{3.7}$$

The momentum conservation in the z direction yields

$$\frac{d\tau_{zx}}{dx} + p_x = 0. \tag{3.8}$$

According to LADM, $\tau_{xz} = -\eta(z)\partial v_z/\partial x$, $\eta(z) = \eta^0[\bar{n}(z)]$. Integrating and applying the no-slip boundary conditions on both walls we get for the velocity profile

$$v_x(z) = p_x \int_{-D/2}^{z} d\xi \frac{\xi}{\eta(\xi)}. \tag{3.9}$$

Note that according to Eq. (3.9) a symmetric density profile leads to a symmetric velocity profile.

The volumetric flow rate is

$$Q = p_x \int_{-D/2}^{D/2} dz \int_{-D/2}^{z} d\xi \frac{\xi}{\eta(\xi)}. \tag{3.10}$$

By rewriting Eq. (3.10) in the form it would have for a homogeneous fluid,

$$Q = -\frac{p_x D^3}{12\eta_{\text{eff}}}. \tag{3.11}$$

We can identify an effective shear viscosity for Poiseuille flow

$$\eta_{\text{eff}} = -\frac{D^3}{12}\left[\int_{-D/2}^{D/2} dz \int_{-D/2}^{z} d\xi \frac{\xi}{\eta(\xi)}\right]^{-1}. \tag{3.12}$$

Note that this is a quite different quantity from the effective viscosity for Couette flow [i.e., Eq. (3.6)].

C. Squeezing flow between parallel circular plates

The hydrodynamic analysis for squeezing flow is considerably more complicated and delicate. A "quasi-steady-state" solution will be used; that is at any time t the radial flow will be treated as a steady-state hydrodynamic problem, but the time rate of change of mass between the two disks will be accounted for properly.[21] For homogeneous fluids this assumption leads to the use of a steady-state equation of continuity. For an inhomogeneous fluid the density at a fixed position in space is a function of the time dependent disk separation as well, i.e.,

$$n = n[z,t,D(t)]. \tag{3.13}$$

If we use the symbol d/dt to denote the time derivative at a fixed position in space the equation of continuity reads

$$\frac{dn}{dt} = \frac{\partial n}{\partial t} + \frac{dD}{dt}\frac{\partial n}{\partial D} = -\frac{\partial}{\partial z}(nv_z) - \frac{1}{r}\frac{\partial}{\partial r}(nrv_r), \tag{3.14}$$

where D is the distance between the plates. The quasi-steady-state approximation amounts to neglecting the term $\partial n/\partial t$. Using also the fact that n is not a function of r we get

$$\frac{dD}{dt}\frac{\partial n}{\partial D} = -\frac{\partial}{\partial z}(nv_z) - n\frac{1}{r}\frac{\partial}{\partial r}(rv_r). \tag{3.15}$$

From Eq. (3.15) and the quasi-steady-state approximation follows that

$$\frac{1}{r}\frac{\partial}{\partial r}(rv_r) = f(z). \tag{3.16}$$

In an inhomogeneous fluid the pressure tensor at equilibrium is not isotropic. Under flow we can always write

$$\mathbf{p} = \mathbf{p}^e + \mathbf{p}^f, \tag{3.17}$$

where the superscripts e and f denote the equilibrium and the flow part of the pressure tensor, respectively. For an inhomogeneous fluid confined between planar micropore walls the condition of hydrostatic equilibrium yields

$$\frac{\partial p^e_{rr}}{\partial r} = 0. \tag{3.18}$$

Using Eqs. (3.17) and (3.18) and neglecting the inertial terms because they are small for squeezing flow[24] if the plates separation is much smaller that the disk radius (a condition that is overwhelmingly satisfied in our case) the momentum balance in the radial direction takes the form

$$-\frac{\partial p^f_{rr}}{\partial r} = \frac{1}{r}\frac{\partial}{\partial r}(r\tau_{rr}) + \frac{1}{r}\frac{\partial \tau_{r\theta}}{\partial \theta} - \frac{\tau_{\theta\theta}}{r} + \frac{\partial \tau_{rz}}{\partial z}. \tag{3.19}$$

According to LADM the stress tensor retains its Newtonian form [Eq. (2.3)]. Using the cylindrical symmetry, neglecting the terms that contain $\nabla\cdot\mathbf{v}$ since they are small for lubrication flows[24] and using Eq. (3.16) the momentum balance reduces to

$$-\frac{\partial p^f_{rr}}{\partial r} = \frac{\partial}{\partial z}\left(\eta(z)\frac{\partial v_r}{\partial z}\right). \tag{3.20}$$

For homogeneous fluids $\partial p^f_{rr}/\partial r = \partial p^f_{zz}/\partial z$ and $\partial p^f_{zz}/\partial z = 0$ if we neglect terms of order D/R and D^2/R^2 in the z equation of motion.[24] In strongly inhomogeneous fluids we know that the equilibrium part of the pressure tensor $\mathbf{p}^e$ is not isotropic and we know nothing about the symmetry properties of the flow part $\mathbf{p}^f$. We cannot, therefore, conclude that p^f_{rr} is z independent from the z independence of p^f_{zz}. We may use, however, a different type of argument. From the equation of continuity (3.15) it follows that $v_r = rg(z)$. Using this fact in the momentum balance equation (3.20) one concludes that $p^f_{rr} = r^2 w(z) + v(z)$. If we require a bulk fluid behavior at the edges of the disks (i.e., p^f_{rr} and $\partial p^f_{rr}/\partial r$ independent of z) we see that p^f_{rr} must be independent of z everywhere. Such an approach cannot obviously account for the complicated edge effects. For disks with radius much larger than the distance between them we expect these effects not to be important, however. Taking advantage of the z independence of p^f_{rr} we can integrate Eq. (3.20) with no slip boundary conditions at $z = \pm D/2$ to get

$$v_r(r,z) = -\frac{dp^f_{rr}}{dr}\int_{-D/2}^{z} \frac{\zeta d\zeta}{\eta(\zeta)}. \tag{3.21}$$

Substituting Eq. (3.21) in the equation of continuity (3.15) integrating and using the impenetrability boundary condition at the lower plate we get

$$v_z(z) = -\frac{1}{n(z)}\left\{\frac{dD}{dt}\int_{-D/2}^{z} d\xi \frac{\partial n(\xi;D)}{\partial D} + \frac{1}{r}\frac{\partial}{\partial r}\left(r dp^f_{rr}/dr\right)\int_{-D/2}^{z} d\xi\, n(\xi) \times \int_{-D/2}^{\xi} d\xi \frac{\xi}{\eta(\xi)}\right\}. \quad (3.22)$$

The impenetrability condition at the upper plate yields

$$v_z(D/2) = \frac{dD}{dt}. \quad (3.23)$$

Applying Eq. (3.22) at $z = D/2$ and using Eq. (3.23) one gets an equation for the pressure $p^f_{rr} = p^f_{rr}(r)$. Integrating, using the boundary condition $p^f_{rr}(R) = p_0$, where R is the radius of the disks, and the requirement that $p^f_{rr}(0)$ be finite, one arrives at the result

$$p^f_{rr} = p_0 + \left[1 - \left(\frac{r}{R}\right)^2\right]\frac{R^2}{4A}\frac{dD}{dt}, \quad (3.24)$$

$$A = \frac{\int_{-D/2}^{D/2} d\zeta\, n(\zeta)\int_{-D/2}^{\zeta} d\xi\,[\xi/\eta(\xi)]}{n_{\text{avg}} + D(\partial n_{\text{avg}}/\partial D)}, \quad (3.25)$$

where n_{avg} is the average density of the whole fluid slab between the plates. This average density n_{avg} depends on the plate separation since the squeezing is supposed to take place under constant chemical potential.[3,11] The disks and the fluid are immersed in a bath containing bulk fluid at constant chemical potential and temperature. To derive Eq. (3.25) we also used the fact that the fluid density exactly on the walls is zero.

By restating Eq. (3.24) in the form it would have for a homogeneous fluid

$$p^f_{rr} = p_0 - 3\left[1 - \left(\frac{r}{R}\right)^2\right]\frac{R^2\eta_{\text{eff}}}{D^3}\frac{dD}{dt} \quad (3.26)$$

we can identify an effective viscosity for squeezing flow:

$$\eta_{\text{eff}} = -\frac{D^3}{12A} = -\frac{D^3}{12}\frac{n_{\text{avg}} + D(\partial n_{\text{avg}}/\partial D)}{\int_{-D/2}^{D/2} dz\, n(z)\int_{-D/2}^{z} d\zeta\,[\zeta/\eta(\zeta)]}. \quad (3.27)$$

Substituting Eq. (3.24) in Eq. (3.21) we get for the radial velocity

$$v_r(r,z) = -\frac{dD}{dt}\frac{r}{2A}\int_{-D/2}^{z} d\zeta \frac{\zeta}{\eta(\zeta)}. \quad (3.28)$$

At the cost of an additional assumption, i.e., that the flow part of the pressure tensor is isotropic ($p^f_{rr} = p^f_{zz}$) we can connect the effective viscosity to a more easily measurable experimental observable, namely the hydrodynamic force exerted on each of the squeezing plates. From Eq. (3.22) and the LADM constitutive equation (2.3) it follows:

$$\tau_{zz} = -2\eta(z)\frac{dD}{dt}\left\{\frac{d}{dz}\left(\frac{1}{n(z)}\right)\left[\frac{\partial}{\partial D}\int_{-D/2}^{z} n(z)dz - \frac{1}{A}\int_{-D/2}^{z} d\zeta\, n(\zeta)\int_{-D/2}^{\zeta} d\xi\frac{\xi}{\eta(\xi)}\right] + \frac{1}{n(z)}\left[-\frac{\partial n(z)}{\partial D} + \frac{1}{A}n(z)\int_{-D/2}^{z}\frac{\zeta d\zeta}{n(\zeta)}\right]\right\}. \quad (3.29)$$

The limiting behavior of the expressions for v_z and τ_{zz} close to the walls needs a careful examination. On a first sight the limits of $v_z(z)$ and $\tau_{zz}(z)$ as $z \to \pm D/2$ (i.e., $n \to 0$) are undetermined quantities. The indeterminacy can be resolved if we apply L'Hôpital's rule and make use of the following conditions:

(1) sufficiently close to the walls the density is very low and thus is proportional to the Boltzmann factor[20] $n \propto \exp\{-[u^e(z) - \mu]/kT\}$;
(2) the density profile close to the walls changes only slightly with wall separation[3,13];
(3) the local viscosity close to the walls changes slowly with z since $\bar{n}(z)$ varies slowly there.

Using all the above we arrive at the results

$$\lim_{z\to -D/2} v_z(z) = 0, \quad \lim_{z\to D/2} v_z(z) = \frac{dD}{dt}, \quad \lim_{z\to -D/2}\tau_{zz} = 0. \quad (3.30)$$

The hydrodynamic force exerted on the lower wall is

$$F_H = \int_0^{2\pi}\int_0^{R}(p^f_{zz} - p_0 + \tau_{zz})_{z=-D/2} r\, dr\, d\theta. \quad (3.31)$$

Using Eqs. (3.30), the assumption $p^f_{zz} = p^f_{rr}$ and Eq. (3.24) we get

$$F_H = \frac{\pi R^4}{8A}\frac{dD}{dt}. \quad (3.32)$$

By rewriting Eq. (3.32) in the homogeneous fluid form,

$$F_H = -\frac{3\pi\eta_{\text{eff}}R^4}{2D^3}\frac{dD}{dt} \quad (3.33)$$

we identify the effective viscosity for squeezing flow with Eq. (3.27) once again. We emphasize, however, that the identification of the effective viscosity with the expression in Eq. (3.27) does not rely on the assumption $p^f_{rr} = p^f_{zz}$ and can be established at an earlier stage.

IV. RESULTS

The units of the various quantities plotted in the following figures are shown in Table I. One of the many density profiles that were determined from the solution of the YBG equation (see Sec. II) is plotted in Fig. 3. Superimposed is the corresponding local average density profile which is related to the actual density profile through Eq. (2.2). The local average density profile also exhibits an oscillatory behavior. Its variation however, is much smoother and its peaks are everywhere lower than $1.0\sigma^{-3}$ a perfectly acceptable homogeneous fluid density since it is everywhere lower than the closest-packing density for a hard sphere fluid $1.41\sigma^{-3}$.[20]

Three velocity profiles for Couette flow and three for

TABLE I. Units of the various quantities.

Length:	σ(molecular diameter)
Mass:	m(molecular mass)
Energy:	$k_B T$
Number density:	σ^{-3}
Velocity:	$(k_B T/m)^{1/2}$
Viscosity:	$\sigma^{-2}(mkT)^{1/2}$
Pressure and shear stress:	$k_B T/\sigma^3$

Poiseuille flow are shown in Figs. 4(a), 4(b), and 4(c) and 5(a), 5(b), and 5(c), respectively. Superimposed are the corresponding density profiles. For the largest wall separation (40σ) the fluid is homogeneous over the middle three quarters of the liquid slab. The velocity profiles in Figs. 4(a) and 5(a) are essentially identical with the ones of a homogeneous fluid. The deviation is much less than that anticipated from the density profile because the local average density, rather than the actual density, is directly related to them. For the other two separations (8σ and 4σ) the density inhomogeneity is very strong and inevitably shows up in the velocity profiles. Nevertheless, the effect of the local density averaging is still apparent. A careful inspection of Figs. 4(b) and 4(c) and 5(b) and 5(c) and a comparison with the homogeneous velocity profiles shows that the shear rate is locally higher than the shear rate occurring in a homogeneous fluid at the same position if the local average density is lower than the pore average density and vice versa. The z dependence of the radial component of the velocity in squeezing flow at a certain radial distance is identical with the Poiseuille flow velocity [see Eqs. (3.9) and (3.28)].

In Fig. 6 the effective viscosities for all three flows are plotted as a function of wall separation. It follows from the whole analysis of flow in strongly inhomogeneous fluids that the effective viscosity is a flow dependent quantity. This is demonstrated by Eqs. (3.6), (3.12), and (3.27), the three definitions of the effective viscosities for the three different flows examined.

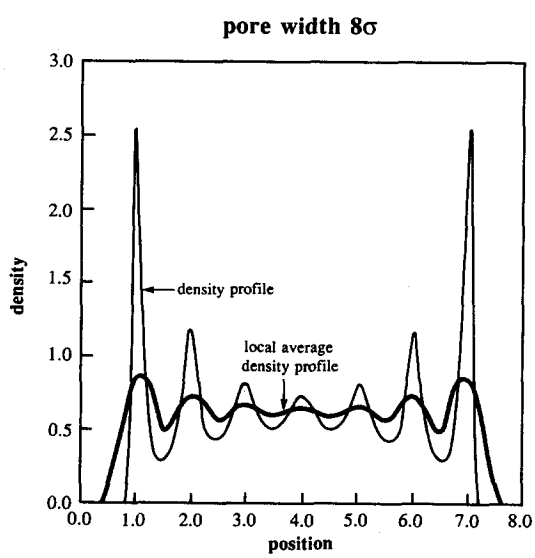

FIG. 3. Density and local average density profiles.

An obvious reason for the effective viscosity variation is the variation of the pore average density with the pore width. The viscosity of a homogeneous fluid with density equal to the pore average density is also shown in Fig. 6. This quantity follows the oscillations of the pore average density.[3] In the limit of large separations the effective viscosities must tend to the homogeneous fluid viscosity, a physical requirement that is obviously satisfied by all three defining equations for the effective viscosities. For smaller separations, however, the behavior of the effective viscosities is characteristic of the flow. The effective viscosity for Poiseuille flow seems to be the most insensitive on the density inhomogeneities. It is indistinguishable from the homogeneous fluid viscosity up to very small separations (6–7σ). The effective viscosity for Couette flow is systematically smaller than the homogeneous fluid viscosity for separations smaller than 20–25σ. At very small separations (less than 4σ) they both become oscillatory functions of the wall separation with period equal to the molecular diameter σ.

The effective viscosity for squeezing flow exhibits a much stranger behavior. Its dependence on the density inhomogeneity is much stronger. Even at separations as large as $\sim 40\sigma$ it is still 10% higher than the homogeneous fluid viscosity. Up to separations 6–7σ it is systematically higher than the homogeneous fluid viscosity. At separations lower than 8σ the effective viscosity for squeezing flow becomes an oscillatory function of the disk separation. The oscillations of this quantity, however, are much stronger and grow much faster as the disks get closer than the ones observed for the effective viscosities for Couette and Poiseuille flow.

Our analysis of flow in strongly inhomogeneous fluids provides for the first time a physical explanation of recent experimental measurements of the effective viscosity of simple nonpolar liquids confined in very narrow spaces.[16,17] These measurements were performed using the surface forces apparatus,[25] an apparatus capable of measuring forces between surfaces separated by very small distances (up to a few Å). In the experiments of Chan and Horn[16] the confined fluid was squeezed between two crossed cylindrical surfaces, whose radii of curvature were much larger than their distance of closest approach. The effective viscosity was found to be systematically higher than the bulk fluid effective vis-

TABLE II. Comparison between LADM predictions and simulation results.

		Effective viscosity	Shear stress
Homogeneous fluid		1.21 ± 0.04	0.181 ± 0.004
Micropore fluid	simulation[a]	0.65 ± 0.02	0.121 ± 0.003
	LADM	0.70	0.130
	usual fluid mechanics	0.38	0.071
	LADM (with local density averaged over 2σ)	0.77	0.143

[a] Reference 14.

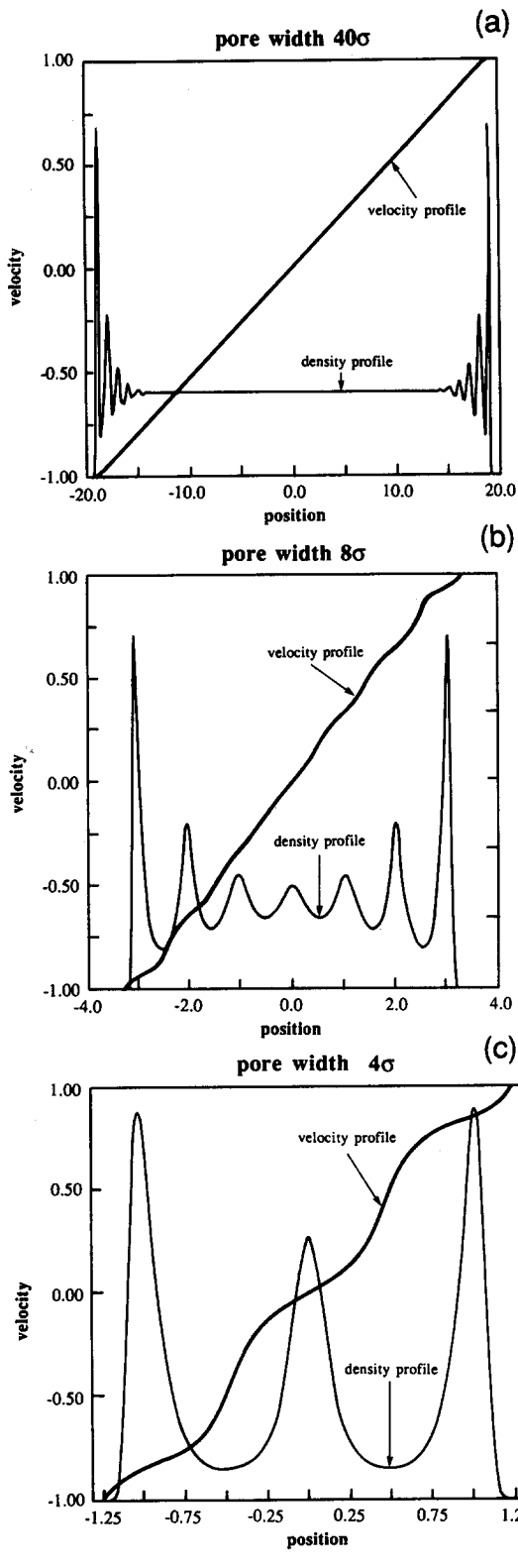

FIG. 4. Velocity profiles for Couette flow: (a) pore width 40σ; (b) pore width 8σ; (c) pore width 4σ.

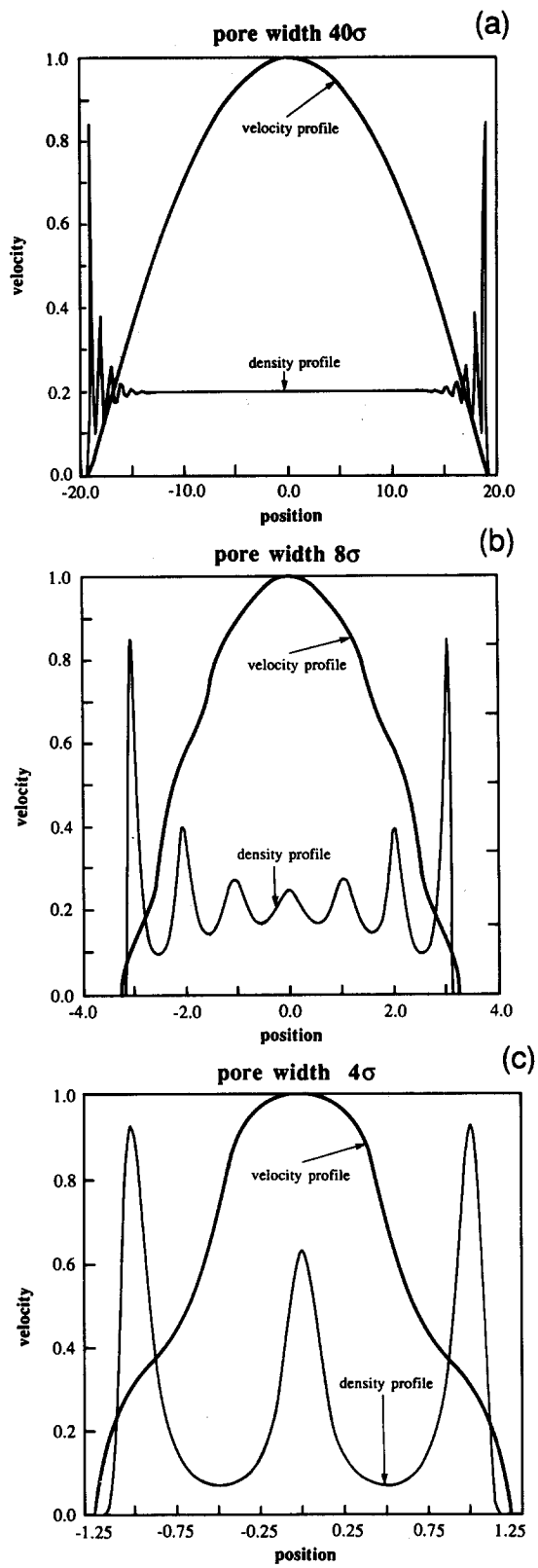

FIG. 5. Velocity profiles for Poiseuille flow: (a) pore width 40σ; (b) pore width 8σ; (c) pore width 4σ.

cosity for separations between 10 and 50 fluid molecular diameters. At smaller separations the cylinder separation was changing in a stepwise manner. In the experiments of Israelachvili a different flow situation was employed, namely the upper cylinder was undergoing forced oscillations along the common normal of the two cylinders. The effective viscosity was found to retain its bulk fluid value up to separations of ten fluid molecular diameters.

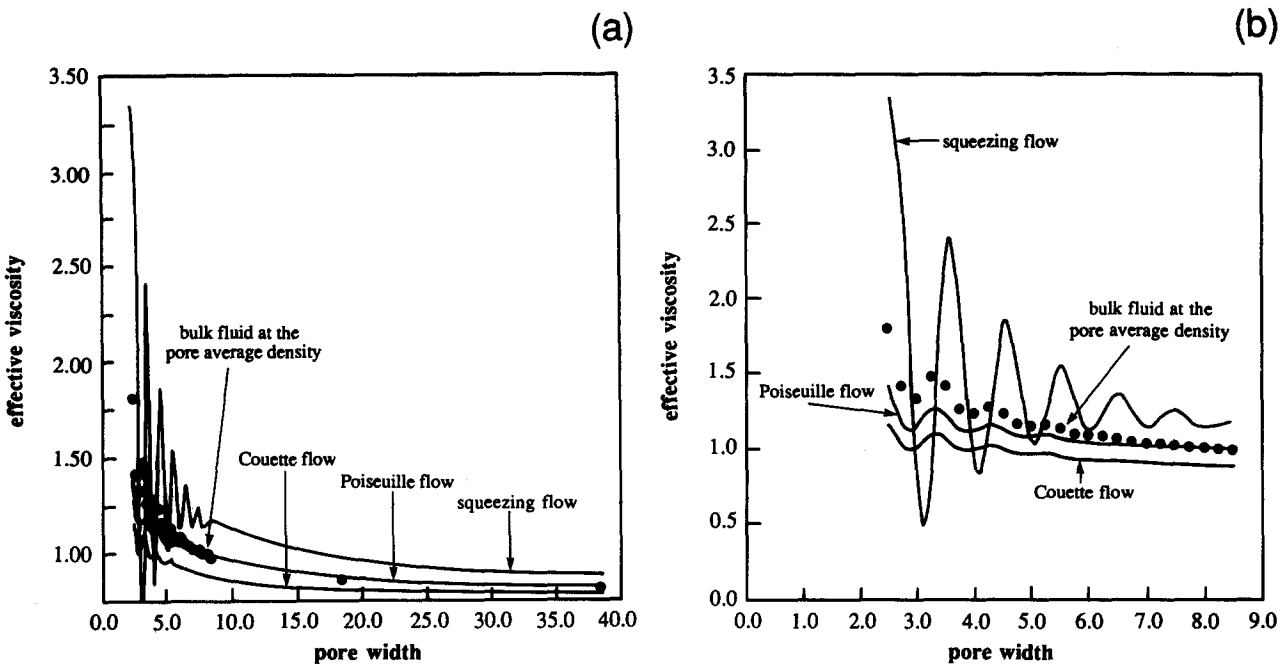

FIG. 6. Effective viscosities for Couette, Poiseuille, and squeezing flows as a function of pore width: (a) range of pore widths 0–40σ; (b) range of pore widths 0–9σ (note that the viscosities are measured in the units of Table I, therefore the bulk fluid viscosity is not 1).

According to our analysis the effective viscosity is a *flow-dependent* quantity. For this reason it is no surprise that two experiments with two different types of flow yielded two different results about the effective viscosity of strongly inhomogeneous fluids. Furthermore, it is not at all clear that the effects of strong density inhomogeneities will already be measurable at ten molecular diameters. This is due to the coarse graining involved in the definition of the local transport coefficients that weakens substantially the spatial variations of the relevant local average density profile.

The squeezing flow between crossed cylinders, examined by Chan and Horn,[16] is similar, although not identical, with the squeezing flow between parallel plates because the radii of curvature of the cylinders were much larger than the distance between them. Our predictions for the effective viscosity in squeezing flow between parallel plates are clearly in qualitative agreement with these experimental findings (see Fig. 6). At separations between 10–40σ our model predicts an effective viscosity higher than the homogeneous fluid viscosity. In Ref. 16 the fluid was found to drain slower than a homogeneous fluid for separations between 10–50 molecular diameters, a fact which implies the existence of an effective viscosity higher than that of the bulk fluid in qualitative agreement with our predictions.

At smaller separations the stepwise change of the separation was entirely attributed to the solvation force between the two cylinders,[4] which is an oscillatory function of separation. Such an approach could not fully explain the experimental findings. The inclusion of the solvation force would produce a stepwise draining but the separations at which the steps were predicted to take place by such an approach did not match those observed experimentally. Our analysis, which leads to an oscillatory effective viscosity and, therefore, an oscillatory hydrodynamic force, suggests that the net force between the cylinders would result from the *interference between two oscillatory terms, namely the solvation force and the hydrodynamic force.* A full comparison, however, with the experimental results, which requires the analysis of the crossed cylinder flow situation employed experimentally, will be the topic of another paper, currently in preparation.

ACKNOWLEDGMENTS

This research was supported in part by grants from the National Science Foundation, the University of Minnesota Supercomputer Institute, the Petroleum Research Fund, the Department of Energy, and by the University of Minnesota Graduate School through Doctoral Dissertation Fellowships awarded to I. Bitsanis and T. K. Vanderlick.

[1] H. T. Davis and L. E. Scriven, Adv. Chem. Phys. **49**, 357 (1982).
[2] I. K. Snook and W. Van Megen, J. Chem. Phys. **72**, 2907 (1980).
[3] J. J. Magda, M. Tirrell, and H. T. Davis, J. Chem. Phys. **83**, 1888 (1985).
[4] R. G. Horn and J. N. Israelachvili, J. Chem. Phys. **75**, 1400 (1981).
[5] S. Nordholm and D. J. Haymet, Aust. J. Chem. **33**, 2013 (1980).
[6] S. Nordholm, M. Johnson, and B. C. Freasier, Aust. J. Chem. **33**, 2139 (1980).
[7] P. Tarazona, Phys. Rev. A **31**, 2672 (1985).
[8] J. Fischer and M. Methfessel, Phys. Rev. A **22**, 2836 (1980).
[9] J. H. Irving and J. G. Kirkwood, J. Chem. Phys. **18**, 817 (1950).
[10] H. T. Davis, J. Chem. Phys. **86**, 1474 (1987).
[11] T. K. Vanderlick and H. T. Davis, J. Chem. Phys. **87**, 1791 (1987).
[12] H. T. Davis, Chem. Eng. Commun. (accepted).
[13] H. T. Davis, I. Bitsanis, T. K. Vanderlick, and M. Tirrell, ACS Symp. Ser. **353**, 257 (1987).
[14] I. Bitsanis, J. J. Magda, M. Tirrell, and H. T. Davis, J. Chem. Phys. **87**, 1733 (1987).
[15] W. T. Ashurst and W. G. Hoover, Phys. Rev. A **11**, 658 (1975).

[16]D. Y. C. Chan and R. G. Horn, J. Chem. Phys. **83**, 5311 (1985).
[17]J. N. Israelachvili, J. Colloid Interface Sci. **110**, 263 (1986).
[18]H. T. Davis, J. Chem. Phys. **85**, 6808 (1986).
[19]K. T. Vanderlick, L. E. Scriven, and H. T. Davis, J. Chem. Phys. (submitted).
[20]D. A. McQuarrie, *Statistical Mechanics* (Harper and Row, New York, 1973).
[21]D. A. Carnahan and K. E. Starling, J. Chem. Phys. **51**, 635 (1969).
[22]W. A. Steele, *The Interaction of Gases with Solid Surfaces* (Pergamon, New York, 1974), Chap. 2.
[23]R. B. Bird, O. Hassager, R. C. Armstrong, and C. F. Curtis, *Dynamics of Polymeric Liquids. Vol. 1. Fluid Mechanics*, 2nd ed. (Wiley, New York, 1987), Chap. 1.
[24]N. Tipei, *Theory of Lubrication* (Stanford University, Stanford, 1962).
[25]J. N. Israelachvili, *Intermolecular and Surface Forces* (Academic, New York, 1985).